

The 750 GeV Boson: Dawn of the Super-Hooperon

Manuel Ernst Krauss^{a,*}, Toby Opferkuch^{a,†}, Florian Staub^{b,‡} and Martin Wolfgang Winkler^{a,§}

^a*Bethe Center for Theoretical Physics & Physikalisches Institut der Universität Bonn,
Nüßallee 12, 53115 Bonn, Germany and*

^b*Theory Department, CERN, 1211 Geneva 23, Switzerland*

We propose a simultaneous explanation of the LHC diphoton excess and the galactic center gamma ray excess within supersymmetry. A gauge singlet, the hooperon, induces the GeV gamma ray signal in the Fermi-LAT data through annihilation into vector-like leptons or quarks. Its scalar superpartner, the super-hooperon, obtains a large diphoton cross section via loops of the same vector-like states. We provide a minimal realization of this scheme within the MSSM extended by a singlet and one vector-like 5-plet of SU(5).

I. INTRODUCTION

In the year 2016, gamma rays provide the most thrilling hints for physics beyond the standard model. An excess of diphotons at the Large Hadron Collider (LHC) [1, 2] might soon turn into the discovery of a new boson with a mass of 750 GeV. Meanwhile, the interpretation of the galactic center gamma ray excess in terms of annihilating dark matter [3] has not lost any of its appeal. In this article we speculate about a possible common origin of both signals within supersymmetry. While a connection has also been discussed within effective field theory in Refs. [4, 5], we go one step further and consider a single superfield which contains both, the 750 GeV boson and the dark matter particle responsible for the galactic center excess.¹ As a possible realization, we study the minimal supersymmetric standard model (MSSM) extended by a singlet and one vector-like 5-plet of SU(5) [13–18]. The vector-like states play a two-fold role: on the one hand, they trigger a large diphoton cross section of the singlet scalar through loop diagrams. On the other hand, they occur as final states in the annihilation of singlet fermion dark matter. Their subsequent decay chain and further fragmentation results in a continuum of gamma rays which is much softer than that of standard model final states. This remains the case even for dark matter masses of order 400 GeV, where the spectrum looks surprisingly similar to the residual spectrum in the galactic center as observed by Fermi-LAT [19]. We show explicitly that there is a parameter region in which both the LHC and Fermi-LAT excesses can be simultaneously explained.

II. THE GALACTIC CENTER GAMMA RAY EXCESS

An excess in the gamma ray flux coming from near the center of the Milky Way was first observed in the Fermi-LAT data by Ref. [3]. In the same work an explanation in terms of annihilating dark matter was proposed and the corresponding particle was soon known as the ‘hooperon’. While subsequent analyses have confirmed the significance of the signal [20–27] the modeling of the diffuse gamma ray emission in the galactic center region remained a source of concern. In Ref. [28] a comprehensive attempt to quantify the systematic uncertainties in the gamma background was made. The excess remained robust against variations in the diffuse emission models. While plausible astrophysical interpretations in terms of millisecond pulsars [29] or cosmic ray bursts [30, 31] have been proposed, dark matter annihilation remains one of the prime explanations of the residual signal – in particular since its morphology matches the expectation from standard dark matter profiles. In Ref. [28] it was realized that the inclusion of systematic errors allows for a harder gamma spectrum compared to the early analyses (see also Ref. [32]). This trend continued with the recently published Fermi-LAT analysis [19] which includes additional systematic uncertainties beyond Ref. [28] in the modeling of the innermost part of the diffuse emission. The Fermi-LAT study was used in Ref. [33] to show that ordinary WIMPs with masses of 35 – 165 GeV can fit the gamma ray excess within uncertainties if they annihilate into bottom quarks². Additionally, dark matter masses of up to 300 GeV became allowed for annihilation into Higgs bosons and top quarks. In this letter we attempt to develop a χ^2 test based on the results of the recent Fermi-LAT analysis. However, before commenting on the specifics of the analysis we begin by determining the gamma-ray flux and illustrating the choices made for the dark matter distribution and associated uncertainties.

The gamma-ray flux arising from self-conjugate dark

* mkrauss@th.physik.uni-bonn.de

† toby@th.physik.uni-bonn.de

‡ florian.staub@cern.ch

§ winkler@th.physik.uni-bonn.de

¹ In Refs. [6–12], the 750 GeV boson was considered as a mediator between dark matter and the standard model.

² In Ref. [33] a preliminary version of the Fermi-LAT analysis was used [34].

matter particles annihilating into all possible final states f in the Galactic dark matter halo can be expressed as

$$\frac{dN}{dE} = \frac{1}{2m_\chi^2} J \sum_f \frac{\langle\sigma v\rangle_f}{4\pi} \frac{dN_f}{dE}. \quad (1)$$

Here, m_χ^2 is the dark matter mass, while $\langle\sigma v\rangle_f$ and dN_f/dE are the velocity averaged annihilation cross-section and the spectra of photons obtained for a given final state f respectively. J , which contains both the line-of-sight and solid angle integrations, is defined through

$$J = \int_{\Delta\Omega} d\Omega \int_{\text{los}} ds \rho(r)^2 \equiv \mathcal{J} J_{\text{can}}, \quad (2)$$

where $\rho(r)$ is the dark matter halo profile centered around the galactic center, $\Delta\Omega$ is the region of interest which for Fermi-LAT is a $15^\circ \times 15^\circ$ box around the galactic center, and s is the line-of-sight.

J_{can} is the central value of J . This quantity corresponds to the central values in the parameters describing the dark matter distribution. Therefore \mathcal{J} parametrizes the uncertainty in the dark matter distribution as a deviation from the canonical profile J_{can} . Here we choose the (generalized) Navarro-Frenk-White (NFW) profile [35]

$$\rho(r) = \rho_0 \frac{(r/r_s)^{-\gamma}}{(1+r/r_s)^{3-\gamma}}, \quad (3)$$

with the canonical profile corresponding to a local dark matter density of $\rho(r_\odot) = 0.4 \text{ GeV/cm}^3$ (where $r_\odot = 8.5 \text{ kpc}$ is the distance between the Sun and the galactic center), scale radius $r_s = 20 \text{ kpc}$ and $\gamma = 1.2$. We follow the analyses of Refs. [28, 33, 36] which estimate the uncertainties to be $\rho(r_\odot) = (0.4 \pm 0.2) \text{ GeV/cm}^3$ and $\gamma = 1.2 \pm 0.1$. This translates into the allowed range of $\mathcal{J} \in [0.14, 4.4]$ with $J_{\text{can}} = 1.08 \times 10^{23} \text{ GeV}^2/\text{cm}^5$.

We now require a goodness-of-fit test for the gamma-ray spectrum based on the results of the Fermi-LAT analysis [19]. In this analysis they developed four specialized models for the diffuse gamma-ray background, which when subtracted from the data all lead to non-negligible residuals. We extracted the spectrum of the excess by subtracting the modeled diffuse gamma-ray background, as given in Fig. 12 and 17 of Ref. [19], from the data. To account for additional systematic uncertainties, we then varied the normalization of the central inverse Compton component by $\pm 50\%$ as motivated by the fits in the Fermi-LAT analysis [19]. Based on the extracted spectra, the mean and variance for each energy bin is determined. The statistical contribution to the variance is estimated from Ref. [34] using the number of events per energy bin. In Fig. 1 we depict the final spectrum of the excess including the derived uncertainties. These are then used to define a χ^2 test statistic.

To validate our interpretation of the Fermi-LAT analysis we perform a $\Delta\chi^2$ fit under the assumption that dark matter annihilates purely to a $b\bar{b}$ final state. This final state is not directly related to our scenario and only

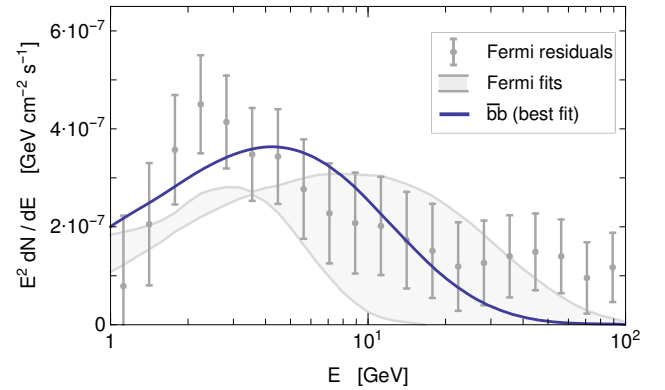


FIG. 1. Energy spectrum of the galactic center gamma ray excess and uncertainties obtained in our analysis. Also shown is the best fit spectrum for dark matter annihilating into bottom quarks and an envelope showing the spread of the Fermi-LAT best-fit exponential cut-off power law spectra.

serves for the comparison with previous analyses. The resulting gamma-ray spectrum as a function of the dark matter mass is taken from Refs. [37, 38]. Utilizing the flux normalization given in Eq. (1), the parameter regions consistent with a $\Delta\chi^2$ at the 1 and 2σ level as well as the best fit point, with $\chi_{\text{min}}^2/\text{d.o.f.} = 0.98$, are shown in Fig. 2. Also shown in this figure are the resulting best fit contours from Ref. [33]. Here the two disconnected contour regions are the result of fitting two different best fit spectra from the Fermi-LAT analysis. The authors argue that the region connecting these two contours is also allowed as each contour represents an extreme choice of the interstellar emission model. By including all diffuse interstellar emission models and varying the inverse Compton component our analysis effectively encompasses uncertainties arising through this choice of model. Also included in Fig. 2 are the limits on the annihilation cross section from dwarf galaxies. For the canonical dark matter profile ($\mathcal{J} = 1$) these exclude the entire parameter space favored by the galactic center excess. However, a slightly steeper profile ($\mathcal{J} \gtrsim 2$) – well within uncertainties – reconciles the excess with the dwarf limits. The spectrum of the best-fit $b\bar{b}$ point (as indicated in Fig. 2) is depicted as a blue line in Fig. 1. In addition we show our derived energy spectrum of the galactic center excess along with an envelope which encompasses the different Fermi-LAT spectra assuming an exponential cut-off power law. These were obtained in Ref. [19] by fitting an excess component with this spectral form to the four mentioned diffuse emission models. While these fits have insufficient spectral freedom to pick up all residuals, it is noted in Ref. [19] that they cannot be ruled out due to the limitations in modeling the interstellar emission. In our goodness-of-fit test they would receive $\chi^2/\text{d.o.f.}$ between 1.1 and 2.1.

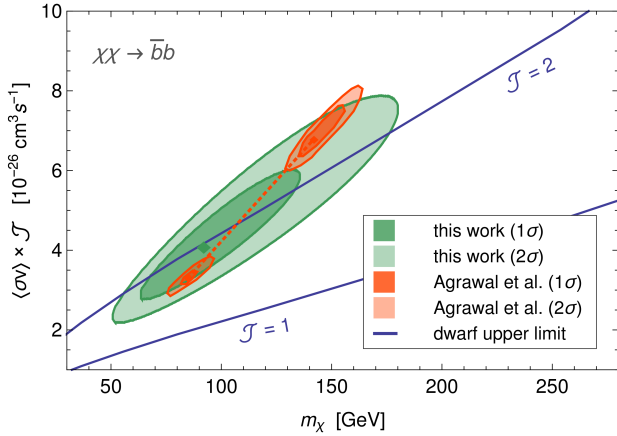


FIG. 2. Parameter regions consistent with the Fermi-LAT gamma-ray excess at 1σ and 2σ . Annihilation of dark matter into bottom quarks is assumed. The green regions refer to our analysis, while the orange regions were obtained in Ref. [33] for two different diffuse emission templates (see text).

III. THE LHC DIPHOTON EXCESS

Preliminary data of the CERN LHC hint at the existence of a new resonance with large diphoton cross section $\sigma_{\gamma\gamma}$ (defined as the product of production cross section and diphoton branching ratio). In this letter we assume a spin 0 resonance produced via gluon fusion and follow the combined likelihood analysis [17] of the ATLAS and CMS 8 + 13 TeV data [1, 2, 39, 40]. For the case of a narrow resonance, the best fit mass $m_\phi = 744$ GeV was identified and

$$\sigma_{\gamma\gamma} = 1.7 - 3.7 \text{ fb} \quad (1.0 - 4.7 \text{ fb}) \quad (4)$$

at the 1σ (2σ) level. The combined local significance of the excess reaches 3.3σ , which can be increased to 3.9σ for two narrow resonances in close proximity. The double resonance is easily realized in supersymmetric models which feature a complex scalar with its components split by loop effects. The simplest and most-widely studied possibility to explain this excess is to generate large couplings between a gauge singlet and two photons/gluons via charged and colored particles in the loop. A comprehensive overview of the proposed models is given in Ref. [41].

IV. A MODEL TO EXPLAIN THE DIPHOTON EXCESS

We consider the MSSM extended by a singlet as well as one copy of vector-like matter superfields transforming as $\mathbf{5} + \bar{\mathbf{5}}$ under $SU(5)$. These contain a lepton-like $SU(2)_L$ doublet, $\hat{L}_5 = (\hat{\nu}_5, \hat{\ell}_5)$, as well as a right-handed down-quark-like superfield, \hat{D}_5 . The corresponding su-

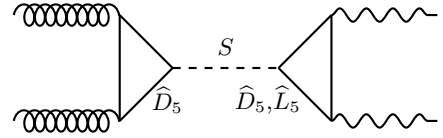


FIG. 3. Schematic diphoton production and decay. The solid lines in the loops stand for both scalar and fermionic components of the superfields \hat{D}_5, \hat{L}_5 .

perpotential reads

$$W = W_{\text{MSSM}} + \frac{\mu_S}{2} \hat{S}^2 + \kappa \hat{S}^3 + (\mu_L + \lambda_L \hat{S}) \hat{L}_5 \hat{L}_5 \quad (5) \\ + (\mu_D + \lambda_D \hat{S}) \hat{D}_5 \hat{D}_5 + Y'_D \hat{D}_5 \hat{Q} \hat{H}_d + Y'_L \hat{E} \hat{L}_5 \hat{H}_d,$$

where we have suppressed color, $SU(2)$ and generation indices. Here, W_{MSSM} denotes the MSSM superpotential and \hat{Q} and \hat{E} the MSSM quark doublet and right-handed charged lepton superfields, respectively. In our notation, hats are assigned to all superfields; in what follows, R -parity-odd fields receive a tilde. Note that, in addition to the superpotentials considered in Refs. [13, 15, 17], we explicitly included the κ and Y' terms. Presence of the Y' couplings avoids a Z_2 symmetry and allows the decay of the otherwise stable vector-like states. In general, the Y' have three entries, but we make the assumption that only the third component is non-vanishing to avoid any limits from flavor changing observables.

For our analysis we have used the *Mathematica* package *SARAH* [42–47] and slightly modified the *NMSSM+VL/5plets* model as provided with Ref. [41]. The interface to the spectrum generator *SPheno* [48, 49] enables the computation of the model-specific full one-loop mass spectrum and dominant two-loop corrections to real scalars [50, 51]. *SARAH/SPheno* has recently been extended for a more precise study of the diphoton excess: for the neutral scalar bosons, in addition to the tree-level decays also the loop-induced decays into two gluons and two photons are calculated, as well as the gluon-fusion production cross-sections at the LHC, both to best-known accuracy. The full model dependent leading order contributions are combined with higher order QCD corrections. For more details, see Ref. [41].

The candidate for the diphoton resonance is the spin-0 part of the singlet superfield, the ‘super-hooperon’, which will be decomposed into its CP-even and CP-odd components h_s and a_s . In the absence of a $\hat{S} \hat{H}_u \hat{H}_d$ term in the superpotential, mixing of the singlets with the MSSM Higgs bosons can be neglected. In Ref. [17] it was found that the LHC diphoton excess is explained in the model under consideration via the diagrams of Fig. 3. While the particles running in the loop for the gluon-fusion production are solely the vector-like (s)quarks stemming from \hat{D}_5 and \hat{D}_5 , the decay diagram also includes the \hat{L}_5 and \hat{L}_5 components.

A necessary condition for a sufficient diphoton rate while being consistent with all existing bounds is that the

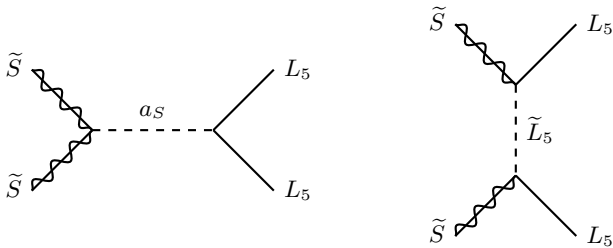


FIG. 4. Relevant diagrams for singlino dark matter annihilation.

vector-like leptons are not substantially heavier than half the resonance mass, therefore maximizing the fermionic loop contributions to the diphoton decay. In addition, the contribution of the CP-even mediator can be enhanced via large supersymmetry-breaking trilinear couplings $T_L \tilde{S} \tilde{L}_5 \tilde{L}_5$ although this possibility is limited by vacuum stability [17, 52]. We further require that the couplings between the singlet and the vector-like fermions remain perturbative up to the scale of grand unification which leads to the constraints $\lambda_D \leq 0.97$ and $\lambda_L \leq 0.63$ at the low scale [13, 17]. We do, however, not impose strict GUT relations on the ratio of vector-like quark and lepton masses allowing them to arise from different unified multiplets as it occurs, e.g. in extradimensional GUTs [13]. With this additional freedom the necessary diphoton cross is obtained within the 1σ uncertainty if only the scalar or the pseudoscalar singlet accounts for the resonance.

V. THE FERMI-LAT EXCESS FROM THE SINGLINO

We consider the scenario where the fermionic superpartner of the 750 GeV boson, \tilde{S} , comprises the dark matter. The by far dominant annihilation final states, if kinematically allowed, are pairs of vector-like leptons or quarks which then further decay via Y'_L, Y'_D . Due to the strong LHC constraints on vector-like quark masses, we will focus on the case where only the vector-like leptons are lighter than \tilde{S} . The annihilation then proceeds via t -channel \tilde{L}_5 exchange and s -channel mediation via the pseudoscalar a_s (see Fig. 4). While for the t -channel exchange, λ_L and the mass of the slepton determine the efficiency of the annihilation, s -channel mediation requires a non-negligible self-coupling κ for the $\tilde{S} \tilde{S} a_s$ vertex.

As the heavy CP even, CP odd and charged MSSM Higgs bosons H, A and H^\pm are typically H_d -like, the dominant decay modes of the final-state vector-like leptons read

$$\ell_5 \rightarrow \tau + H/A, \quad (6)$$

$$\nu_5 \rightarrow \tau^\mp + H^\pm, \quad (7)$$

with a branching ratio of about 70% and more if they are kinematically accessible. Other final states include

the light Higgs h or electroweak gauge bosons. We assumed that L_5 only couples to the third generation of MSSM leptons. The heavy MSSM Higgs bosons further decay as $H/A \rightarrow b\bar{b}$ and $H^\pm \rightarrow tb$. Therefore, it is mainly the masses m_{L_5} and m_A which fix the gamma ray spectrum.

For the calculation of the spectrum as well as the dark matter relic density, we use `MicrOMEGAs-4.2.5` [53–58] through the interface with `SARAH`. As the annihilation does not involve highly energetic electrons or muons, we neglect bremsstrahlung and inverse Compton contributions.³ The dark matter distribution is modeled with the NFW profile as described in Eq. 3.

In order to match the Fermi-LAT excess the spectrum should be rather soft, peaking at GeV energies, see Fig. 1. This is a non-trivial constraint as an explanation to the LHC diphoton excess requires $m_{L_5} \gtrsim 375$ GeV, such that the tree-level decay of the resonance into vector-like leptons is forbidden. Thus, even if dark matter is only slightly heavier than m_{L_5} the vector-like lepton decay leads to a strong energy release. Fortunately this energy is distributed between a large number of final states. Viable spectra can be obtained as long as the decay dominantly proceeds via intermediate heavy Higgs bosons which requires $m_{L_5} - m_A \gtrsim 20$ GeV to avoid phase space suppression. The differential gamma ray fluxes for three different values of m_A and fixed $m_{L_5} = 375$ GeV, $m_{\tilde{S}} = 384$ GeV are shown in Fig. 5. The goodness-of-fit to the galactic center excess is obtained from our χ^2 measure as described in Section II. The overall normalization factor \mathcal{J} of each spectrum is chosen to minimize χ^2 . The best fit with $\chi^2/\text{d.o.f.} = 1.02$ is obtained for the intermediate mass $m_A = 334$ GeV. For larger $m_A = 356$ GeV, decay chains involving vector bosons or the light Higgs⁴ become significant. The fit gets worse due to the shoulder towards higher energies which results from the relatively highly-boosted tau in the final state. A shoulder is also developed for smaller $m_A = 300$ GeV which again leaves more phase space for the τ . Small $m_A \lesssim 300$ GeV is, furthermore, excluded by LHC Higgs searches in the $\tau\tau$ -channel [59] for the chosen $\tan\beta$ value of 7.⁵

While the best spectrum ($m_A = 334$ GeV) falls into the 1σ range of our goodness-of-fit test it appears not to capture the residual spectrum at $E \lesssim 2$ GeV very well. However, it should be noted that gamma ray spectra from dark matter annihilation rather generically take the (approximate) form of an exponential cut-off power law [33]. As mentioned, Fermi has provided best fit spectra of this form for their different diffuse background models, their envelope is also shown in Fig. 5. It can be seen that our spectra are very similar to the best exponential cut-off

³ These contributions could become important if Y'_L contained non-vanishing first or second entries opening the decay of L_5 into electrons or muons.

⁴ The light Higgs mass is adjusted to ~ 125 GeV by the stop sector.

⁵ We use the tool `HiggsBounds` [60–62] to check these limits.

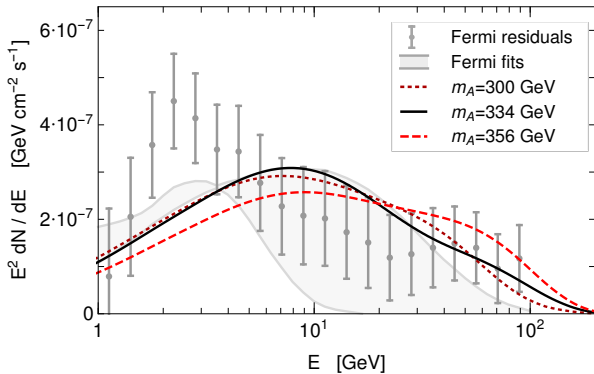


FIG. 5. Energy spectrum of the galactic center gamma rays from singlino dark matter with $m_{\tilde{S}} = 384$ GeV annihilating into $L_5\bar{L}_5$ with $m_{L_5} = 375$ GeV for different masses of A . Also shown are the residuals as obtained in Section II as well as the envelope of the Fermi-LAT best-fit spectra assuming an exponential cut-off power law spectrum.

power laws. Clearly, one can find dark matter spectra which fit the low energy part of the excess better than ours, but the trade-off is then typically a worse fit at higher energies (as e.g. in the case of annihilation into bottom quarks, see Fig. 2).

Let us now turn to the normalization of the spectrum. To make the singlet fermion a thermal dark matter candidate its freeze-out cross section must be $\langle\sigma v\rangle_{\text{FO}} = 2 - 3 \times 10^{-26} \text{ cm}^3/\text{s}$. Assuming the domination of t -channel \tilde{L}_5 exchange as shown in the right panel of Fig. 4, today's annihilation cross section turns out to be of the same size. This results in a normalization of the gamma ray spectrum which is too low unless one invokes $\mathcal{J} \sim 10$ in Eq. 1. This is beyond the range of $\mathcal{J} \in [0.14, 4.4]$ we consider as realistic. If one is not willing to push astrophysical uncertainties, e.g. by invoking more strongly contracted dark matter profiles, one needs to resort to mechanisms that enhance today's annihilation cross section over the one at freeze-out. In the following we discuss two explicit mechanisms which result in Ωh^2 within the measured range [63] as well as a normalization of the gamma spectrum with $\mathcal{J} \lesssim 4$: bino coannihilation and a pseudoscalar resonance.

Bino coannihilation For a small mass splitting ΔM between the \tilde{S} and the bino \tilde{B} , coannihilation gets important for the thermal cross section. As the bino interacts weaker than the singlino, this will in total reduce $\langle\sigma v\rangle_{\text{FO}}$, effectively enhancing the relic density without changing today's annihilation $\langle\sigma v\rangle$. Thus, for sufficiently small ΔM it is possible to find parameter regions with $\langle\sigma v\rangle/\langle\sigma v\rangle_{\text{FO}} \sim 3 - 5$. In Fig. 6 we show the result of a scan over m_A and ΔM while keeping $m_{\tilde{S}} = 387$ GeV and $\Omega h^2 \approx 0.12$ fixed through adapting λ_L . The galactic center excess is fit within 1σ for mass splittings up to $\Delta M \sim 2.5$ GeV and $m_A = 310 - 360$ GeV if we require $\mathcal{J} \leq 4.4$. The lower bound on m_A arises from Higgs

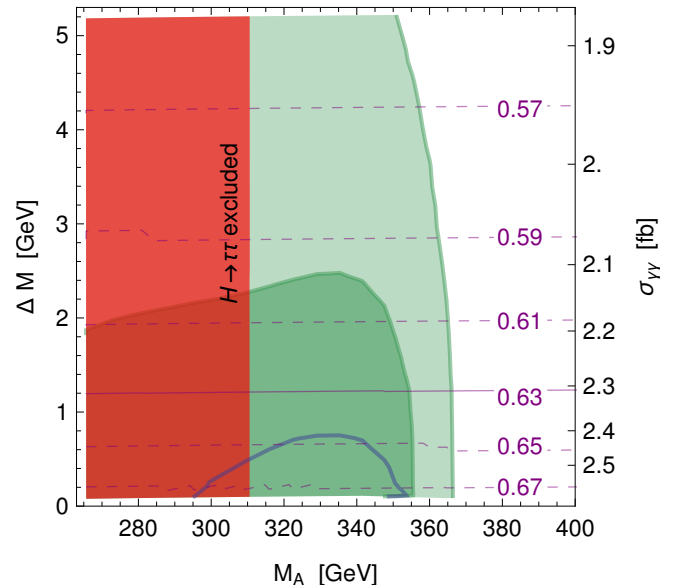


FIG. 6. Parameter scan indicating gamma ray spectra which fit the galactic center excess at 1σ (dark green) and 2σ (light green) depending on the MSSM pseudoscalar mass and the bino-singlino mass splitting. We set $m_{\tilde{S}} = 387$ GeV, $m_{L_5} = 382$ GeV, $m_{\tilde{L}_{5,1,2}} \approx 500$ GeV, $\tan\beta = 7.5$, $\kappa = 0$. The relic density is fixed at $\Omega h^2 \approx 0.12$ by adjusting the coupling λ_L as indicated by the purple contours. On the right y -axis we show the diphoton cross section at 13 TeV from the added signals of h_s and a_s . The area marked in red is in conflict with LHC searches for a heavy Higgs decaying to $\tau\tau$ [59]. The blue contour at the bottom would be obtained if the current gamma ray limits from dwarf galaxies became stronger by 50%.

searches, the upper bound from the required shape of the gamma ray spectrum. In addition, a part of the parameter space at $\lambda_L > 0.63$ is excluded by requiring perturbativity up to the GUT scale. Gamma ray limits from dwarf galaxies are close in sensitivity but do not yet lead to an exclusion (see Fig. 6).⁶ The diphoton cross section varies with λ_L , but falls into the 1σ range of the LHC diphoton excess over the entire depicted range.

Pseudoscalar resonance A further possibility to enhance $\langle\sigma v\rangle/\langle\sigma v\rangle_{\text{FO}}$ opens up near the pseudoscalar s -channel resonance if the mass splitting $m_{a_s} - 2m_{L_5}$ is sufficiently small: while today's annihilation cross section $\tilde{S}\tilde{S} \rightarrow a_s$ peaks at $m_{\tilde{S}} = m_{a_s}/2$, the thermal cross section already peaks at slightly smaller dark matter masses due to the higher momentum in the early universe. Be-

⁶ The limits on the gamma ray spectrum from dwarf galaxies are only available for limited types of dark matter annihilation final states like $b\bar{b}$ and W^+W^- . As the latter spectrum is most similar in shape to our scenario, we infer the corresponding bounds by fitting our spectrum to a WW spectrum with free dark matter mass and annihilation cross section.

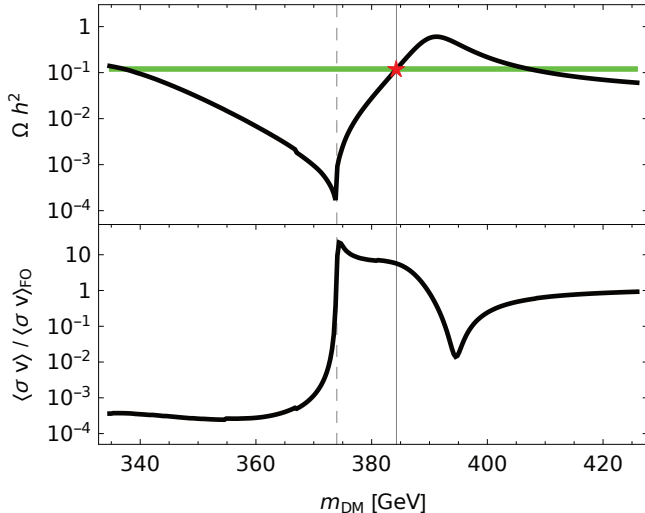


FIG. 7. Dependence of the relic density and the ratio of velocity-averaged annihilation cross sections today and at freeze-out on the mass of the singlino with fixed $m_{a_s} = 748$ GeV and $m_{L_5} = 374.5$ GeV, using $\kappa = 2.4 \cdot 10^{-2}$, $m_A = 334$ GeV, $\tan\beta = 7$, $\lambda_L = 0.63$. The green line indicates the observed dark matter relic density.

cause of this relative shift of the peaks, today’s annihilation cross section is enhanced with respect to the one at the time of freeze-out for $m_{\tilde{S}} \gtrsim m_{a_s}/2$. In Fig. 7 we scan the singlino mass around $m_{a_s}/2$. We show the relic density as well as $\langle\sigma v\rangle/\langle\sigma v\rangle_{\text{FO}}$ as a function of the singlino mass using $\kappa = 2.4 \cdot 10^{-2}$. The apparent broad width of the resonance at lower masses is due to the open decay channels $a_s \rightarrow \tilde{S}\tilde{S}$. Above the resonance, where $\langle\sigma v\rangle/\langle\sigma v\rangle_{\text{FO}}$ reaches its maximal value, the a_s decay into two singlinos is forbidden but $a_s \rightarrow L_5\bar{L}_5$ opens up. Our benchmark point with the correct dark matter density is marked by the solid gray line, indicating a relative cross-section enhancement of $\langle\sigma v\rangle/\langle\sigma v\rangle_{\text{FO}} \approx 5$ and corresponding to $\chi^2/\text{d.o.f.} = 1.02$. This point leads to the gamma spectrum shown by the black line in Fig. 5, and results in a diphoton cross section at LHC-13 of 2.45 fb. For singlino masses around 390 GeV, a destructive interference between the s - and t -channel diagrams leads to a small peak (dip) in Ωh^2 (the cross section ratio). At higher dark matter masses, the annihilation mechanism is again dominated by the \tilde{L}_5 t -channel and $\langle\sigma v\rangle/\langle\sigma v\rangle_{\text{FO}}$ approaches unity.

We additionally remark that this scenario of resonant enhancement can also be realized at higher masses of $m_{a_s} > 750$ GeV $> 2m_{L_5}$. In this case, the diphoton cross section must be exclusively contributed by h_s , which is realizable by large trilinear couplings to the vector-like sleptons. The pseudoscalar a_s , in turn, almost exclusively decays into on-shell $L_5\bar{L}_5$ and is therefore not yet detectable at the LHC.

We have checked that the monochromatic diphoton line which is emitted by singlino annihilation at loop order is consistent with existing bounds [64]. In addition, we have used MicrOMEGAS to calculate the dark matter induced antiproton flux taking propagation parameters from the recent boron to carbon analysis [65]. The predicted flux is not excluded but close to the sensitivity of AMS-02 [66].

In the upshot, the Fermi and LHC excesses can be explained simultaneously with the dark matter produced by ordinary thermal freeze-out.

VI. CONCLUSION

In this letter we proposed an intimate connection between the LHC diphoton excess and the galactic center gamma ray excess within supersymmetry. In our scheme, the 750 GeV boson and the ‘hooperon’ are the scalar and fermionic manifestations of the same singlet superfield. The latter couples to new vector-like degrees of freedom which mediate the diphoton decay of the scalar and, at the same time, occur as final states in the annihilation of the (dark matter) fermion. To retain the desirable feature of gauge coupling unification, we assumed the vector-like states populate the $\mathbf{5}$ and $\bar{\mathbf{5}}$ representation of SU(5). The LHC diphoton excess is explained within 1σ for a vector-like lepton mass $\lesssim 400$ GeV and quark mass $\lesssim 800$ GeV. The singlino which we take to be in the mass range of 380 – 500 GeV naturally obtains a relic density $\Omega h^2 \simeq 0.12$ through standard thermal freeze-out. The vector-like leptons which occur as final states in its annihilation induce a rather soft gamma ray continuum through their long decay chains, in particular if the latter involve heavy MSSM Higgs bosons. For heavy Higgs masses of 300–400 GeV the spectrum is soft enough to fit the galactic gamma ray excess within astrophysical uncertainties. The correct normalization of the gamma ray signal requires either a rather steep dark matter profile, or a slight enhancement of the annihilation cross section today compared to the early universe. We provided simple thermal mechanisms leading to this result. The model we described is highly testable. Apart from new vector-like quarks and leptons close to the current experimental limits, it predicts the discovery of the heavy MSSM Higgs boson in the $\tau\tau$ channel at LHC-13.

ACKNOWLEDGEMENTS

We would like to thank Hans Peter Nilles and Matthew McCullough for interesting discussions as well as Herbi Dreiner for helpful comments on the manuscript. MEK is supported by the DFG Research Unit 2239 “New Physics at the LHC”, MWW by the SFB-Transregio TR33 “The Dark Universe”.

-
- [1] ATLAS, ATLAS-CONF-2015-081 (2015).
- [2] CMS, CMS-PAS-EXO-15-004 (2015).
- [3] L. Goodenough and D. Hooper, (2009), 0910.2998.
- [4] X.-J. Huang, W.-H. Zhang, and Y.-F. Zhou, (2015), 1512.08992.
- [5] A. Hektor and L. Marzola, (2016), 1602.00004.
- [6] Y. Mambrini, G. Arcadi, and A. Djouadi, *Phys. Lett. B* **755**, 426 (2016), 1512.04913.
- [7] M. Backovic, A. Mariotti, and D. Redigolo, *JHEP* **03**, 157 (2016), 1512.04917.
- [8] C. Han, H. M. Lee, M. Park, and V. Sanz, *Phys. Lett. B* **755**, 371 (2016), 1512.06376.
- [9] M. Bauer and M. Neubert, (2015), 1512.06828.
- [10] J.-C. Park and S. C. Park, (2015), 1512.08117.
- [11] K. Ghorbani and H. Ghorbani, (2016), 1601.00602.
- [12] V. De Romeri, J. S. Kim, V. Martin-Lozano, K. Rolbiecki, and R. R. de Austri, (2016), 1603.04479.
- [13] L. J. Hall, K. Harigaya, and Y. Nomura, *JHEP* **03**, 017 (2016), 1512.07904.
- [14] Y.-L. Tang and S.-h. Zhu, (2015), 1512.08323.
- [15] B. Dutta *et al.*, (2016), 1601.00866.
- [16] R. Barbieri, D. Buttazzo, L. J. Hall, and D. Marzocca, (2016), 1603.00718.
- [17] H. P. Nilles and M. W. Winkler, (2016), 1604.03598.
- [18] L. J. Hall, K. Harigaya, and Y. Nomura, (2016), 1605.03585.
- [19] Fermi-LAT, M. Ajello *et al.*, *Astrophys. J.* **819**, 44 (2016), 1511.02938.
- [20] D. Hooper and L. Goodenough, *Phys. Lett. B* **697**, 412 (2011), 1010.2752.
- [21] D. Hooper and T. Linden, *Phys. Rev. D* **84**, 123005 (2011), 1110.0006.
- [22] K. N. Abazajian and M. Kaplinghat, *Phys. Rev. D* **86**, 083511 (2012), 1207.6047, [Erratum: *Phys. Rev. D* **87**, 129902(2013)].
- [23] D. Hooper and T. R. Slatyer, *Phys. Dark Univ.* **2**, 118 (2013), 1302.6589.
- [24] C. Gordon and O. Macias, *Phys. Rev. D* **88**, 083521 (2013), 1306.5725, [Erratum: *Phys. Rev. D* **89**, no.4, 049901(2014)].
- [25] K. N. Abazajian, N. Canac, S. Horiuchi, and M. Kaplinghat, *Phys. Rev. D* **90**, 023526 (2014), 1402.4090.
- [26] T. Daylan *et al.*, *Phys. Dark Univ.* **12**, 1 (2016), 1402.6703.
- [27] B. Zhou *et al.*, *Phys. Rev. D* **91**, 123010 (2015), 1406.6948.
- [28] F. Calore, I. Cholis, and C. Weniger, *JCAP* **1503**, 038 (2015), 1409.0042.
- [29] K. N. Abazajian, *JCAP* **1103**, 010 (2011), 1011.4275.
- [30] E. Carlson and S. Profumo, *Phys. Rev. D* **90**, 023015 (2014), 1405.7685.
- [31] J. Petrovi, P. D. Serpico, and G. Zaharija, *JCAP* **1410**, 052 (2014), 1405.7928.
- [32] T. Linden, N. L. Rodd, B. R. Safdi, and T. R. Slatyer, (2016), 1604.01026.
- [33] P. Agrawal, B. Batell, P. J. Fox, and R. Harnik, *JCAP* **1505**, 011 (2015), 1411.2592.
- [34] Fermi-LAT, S. Murgia, (2014), http://fermi.gsfc.nasa.gov/science/mtgs/symposia/2014/program/08_Murgia.pdf.
- [35] J. F. Navarro, C. S. Frenk, and S. D. M. White, *Astrophys. J.* **462**, 563 (1996), astro-ph/9508025.
- [36] F. Iocco, M. Pato, G. Bertone, and P. Jetzer, *JCAP* **1111**, 029 (2011), 1107.5810.
- [37] M. Cirelli *et al.*, *JCAP* **1103**, 051 (2011), 1012.4515, [Erratum: *JCAP* **1210**, E01(2012)].
- [38] P. Ciafaloni *et al.*, *JCAP* **1103**, 019 (2011), 1009.0224.
- [39] ATLAS, G. Aad *et al.*, *Phys. Rev. Lett.* **113**, 171801 (2014), 1407.6583.
- [40] CMS, V. Khachatryan *et al.*, *Phys. Lett. B* **750**, 494 (2015), 1506.02301.
- [41] F. Staub *et al.*, (2016), 1602.05581.
- [42] F. Staub, (2008), 0806.0538.
- [43] F. Staub, *Comput. Phys. Commun.* **181**, 1077 (2010), 0909.2863.
- [44] F. Staub, *Comput. Phys. Commun.* **182**, 808 (2011), 1002.0840.
- [45] F. Staub, *Computer Physics Communications* **184**, pp. 1792 (2013), 1207.0906.
- [46] F. Staub, *Comput. Phys. Commun.* **185**, 1773 (2014), 1309.7223.
- [47] F. Staub, *Adv. High Energy Phys.* **2015**, 840780 (2015), 1503.04200.
- [48] W. Porod, *Comput. Phys. Commun.* **153**, 275 (2003), hep-ph/0301101.
- [49] W. Porod and F. Staub, *Comput. Phys. Commun.* **183**, 2458 (2012), 1104.1573.
- [50] M. D. Goodsell, K. Nickel, and F. Staub, *Eur. Phys. J. C* **75**, 32 (2015), 1411.0675.
- [51] M. Goodsell, K. Nickel, and F. Staub, *Eur. Phys. J. C* **75**, 290 (2015), 1503.03098.
- [52] A. Salvio, F. Staub, A. Strumia, and A. Urbano, *JHEP* **03**, 214 (2016), 1602.01460.
- [53] G. Belanger, F. Boudjema, A. Pukhov, and A. Semenov, *Comput. Phys. Commun.* **149**, 103 (2002), hep-ph/0112278.
- [54] G. Belanger, F. Boudjema, A. Pukhov, and A. Semenov, *Comput. Phys. Commun.* **174**, 577 (2006), hep-ph/0405253.
- [55] G. Belanger, F. Boudjema, A. Pukhov, and A. Semenov, *Comput. Phys. Commun.* **176**, 367 (2007), hep-ph/0607059.
- [56] G. Belanger, F. Boudjema, A. Pukhov, and A. Semenov, *Comput. Phys. Commun.* **180**, 747 (2009), 0803.2360.
- [57] G. Belanger, F. Boudjema, A. Pukhov, and A. Semenov, *Comput. Phys. Commun.* **185**, 960 (2014), 1305.0237.
- [58] G. Blanger, F. Boudjema, A. Pukhov, and A. Semenov, *Comput. Phys. Commun.* **192**, 322 (2015), 1407.6129.
- [59] CMS, CMS-PAS-HIG-14-029 (2015).
- [60] P. Bechtle, O. Brein, S. Heinemeyer, G. Weiglein, and K. E. Williams, *Comput. Phys. Commun.* **181**, 138 (2010), 0811.4169.
- [61] P. Bechtle, O. Brein, S. Heinemeyer, G. Weiglein, and K. E. Williams, *Comput. Phys. Commun.* **182**, 2605 (2011), 1102.1898.
- [62] P. Bechtle *et al.*, *Eur. Phys. J. C* **74**, 2693 (2014), 1311.0055.
- [63] Planck, P. A. R. Ade *et al.*, *Astron. Astrophys.* **571**, A16 (2014), 1303.5076.
- [64] Fermi-LAT, M. Ackermann *et al.*, *Phys. Rev. D* **91**, 122002 (2015), 1506.00013.

- [65] R. Kappl, A. Reinert, and M. W. Winkler, JCAP **1510**, 034 (2015), 1506.04145.
- [66] AMS, A. Kounine, (2015), http://indico.cern.ch/event/381134/contributions/900587/attachments/759339/1041605/AMS_positrons_antiprotons.pdf.